Flexible Organic/Inorganic Hybrid Near-Infrared Photoplethysmogram Sensor for Cardiovascular Monitoring

*Huihua Xu, Jing Liu, Jie Zhang, Guodong Zhou, Ningqi Luo, and Ni Zhao**

Wearable photoplethysmogram (PPG) sensors offer convenient and informative measurements for evaluating daily physiological states of individuals. In this work, epidermal and flexible near-infrared (NIR) PPG sensors integrating a low-power, high-sensitivity organic phototransistor (OPT) with a high-efficiency inorganic light-emitting diode are developed. By exploiting an organic bulk heterojunction active layer and a bilayer gate dielectric design, a low voltage (<3 V) operated OPT with NIR responsivity as high as 3.5×10^5 A W^{-1} and noise equivalent power of 1.2×10^{-15} W $Hz^{-1/2}$ is achieved, greatly surpassing commercial available silicon-based photodetectors. In addition, the ultrathin encapsulation structure renders the device highly flexible and allows transfer printing of the device directly onto human skin. It is demonstrated that the epidermal/flexible PPG sensors are capable of continuously monitoring heart rate variability and precisely tracking the changes of pulse pressure at different postures of human subjects with the aid of electrocardiogram monitoring, exhibiting more reliable performance than commercial PPG sensors while consuming less power. The study suggests that the hybrid PPG sensor design may provide a promising solution for low-power, real-time physiological monitoring.

With the growing aging population and prevalence of cardiovascular diseases (CVDs), there is an increasing demand for developing personal healthcare systems that can frequently collect physiological parameters of patients during their daily life, thus allowing early disease detection and timely response of health treatments. Continuous monitoring of cardiovascular parameters, including heart rate (HR),[1] heart rate variability (HRV),[2] and blood pressure (BP),[3] is of great importance for the prognosis and diagnosis of CVDs—the leading global cause of death.[4] Accordingly, wearable medical electronics have been proposed owing to their capability of continuously monitoring the physiological conditions of individuals without constraints on time and place.

Among various monitoring techniques, photoplethysmogram (PPG)[5] is widely used to predict vital health concerned parameters such as heart pulsation and arterial blood pressure (by using together with electrocardiogram (ECG)).[6] When used in a multiwavelength configuration,[5a–c] it can also measure blood oxygen level and hemodynamic responses, a function that cannot be realized with mechanical pulse sensors.[7] The key components of a PPG sensor include a light-emitting diode (LED) and a photodetector applied to the skin. The light emitted from the LED is partially absorbed and scattered in the tissue; then the reflected or transmitted light is measured by the photodetector, which can be placed either beside or opposite the LED (corresponding to reflection and transmission mode PPG sensors, respectively). During a systolic and diastolic process both the optical density and path length of the illuminated tissue are changing (due to the variation in the orientation and concentration of erythrocytes and the light-absorbing hemoglobin they carry). Consequently, the intensity of the reflected or transmitted light varies according to the arterial pulse wave. Currently, the commercially available PPG sensors are assembled following the traditional designs of integrated circuit (IC) technologies and are bulky and rigid. This could limit the accuracy of the physiologic information extractable from the sensor output when the wearer is in motion or when there is strong ambient light noise. High power consumption is another critical issue. To improve the signal-to-noise ratio, relatively high power LEDs are used, which imposes a demand on frequent charging of the PPG devices.

To address the rigidity issue of the PPG sensors, organic thin-film devices have been explored recently. Organic light-emitting diodes (OLEDs) and organic photodiodes (OPDs) were fabricated on plastic substrates and paired up to form a transmission- or reflection-mode all-organic optoelectronic sensors for pulse oximetry[5b,c,8] and muscle contraction sensing[5d] applications. The all-organic devices provide great flexibility and conformality to skin; however, they are operated in the visible spectral range (e.g., green and red) so far. This imposes a limitation on the penetration depth of light into the skin tissue. As shown in Figure S1 (Supporting Information), the vascular tree in the skin consists of arteries, arterioles, and capillaries, where the blood flow is pumped through in sequence. In arterial pulsation measurements, e.g., BP estimation, a longer wavelength PPG light probe, such as red or near infrared (NIR), is often used because the long wavelength light has a deeper penetration depth into skin and is capable of picking up signals from the larger arterioles and possibly arteries in the deep dermis.[9] In addition to penetration depth, light attenuation also needs

Dr. H. Xu, J. Liu, Dr. J. Zhang, G. Zhou, N. Luo, Prof. N. Zhao
Department of Electronic Engineering
The Chinese University of Hong Kong
New Territories, Hong Kong SAR, China
E-mail: nzhao@ee.cuhk.edu.hk

DOI: 10.1002/adma.201700975

to be taken into account. Red light is significantly attenuated while traveling through the skin and tissue, whereas NIR light can be more efficiently transmitted, enabling signal collection from a wider region.

In this work, we demonstrate epidermal and flexible PPG sensors that can be operated in the NIR regime with high sensitivity and low power consumption. The PPG sensor hybrids an organic phototransistor (OPT) with an inorganic light-emitting diode (Model ED-B42IRT-RS from OPTOTECH). The model ED-B42IRT-RS offers much higher power conversion efficiency (14.3%) as compared to NIR OLEDs,[10] and it can be easily bonded to flexible substrates through transfer printing. By combining a bulk heterojunction active layer with high-k gate dielectric, we have achieved a low voltage (<3 V) operated OPT with NIR responsivity as high as 3.5×10^5 A W^{-1} and noise equivalent power of 1.2×10^{-15} W Hz$^{-1/2}$, largely surpassing the performance of commercially available silicon photodiodes. Sandwiched between ultrathin polymer encapsulation layers, the OPT exhibits good air stability and mechanical flexibility, and can be intimately and unobtrusively attached to the skin for physiological signal monitoring. To demonstrate the practical applications of the devices, we developed an epidermal and a flexible PPG sensor for HRV and BP measurements, respectively. Compared to commercial PPG sensors, our PPG sensor probe allows lower power consumption due to the combination of the low-voltage, high-sensitivity OPT, and high-efficiency LED and is capable of detecting cardiovascular signal accurately due to intimate contact with the skin.

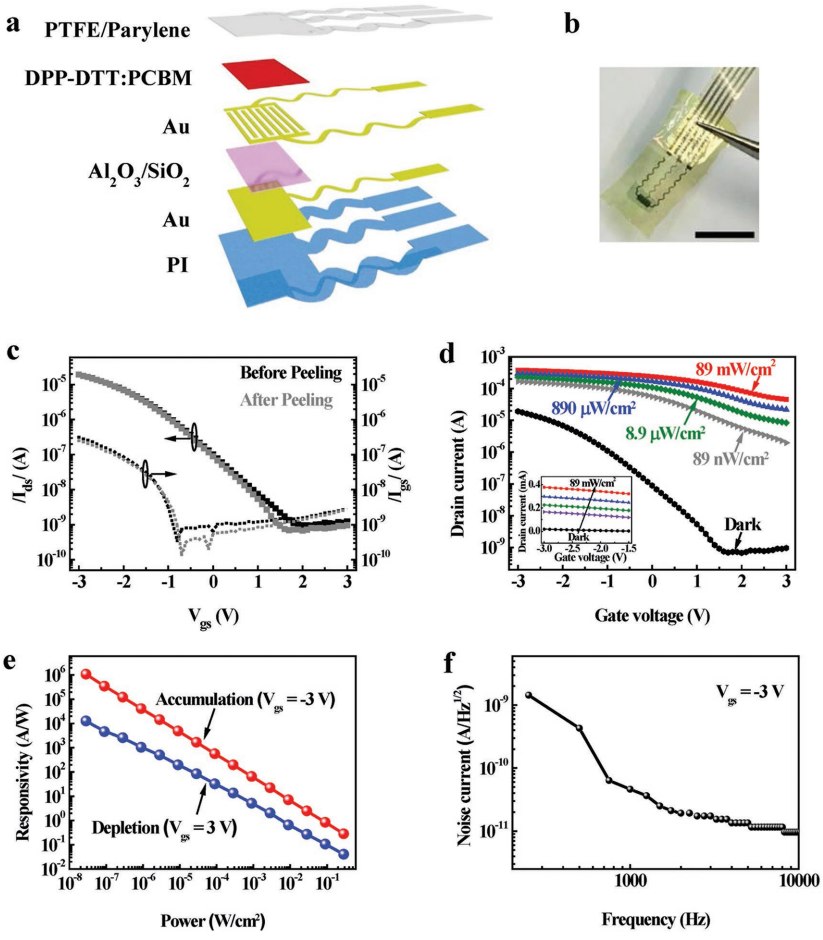

Figure 1. Characteristics of flexible OPTs. a) Schematic of the device structure of the flexible OPT. b) Picture of a freestanding OPT (Scale bar, 5 mm). c) Transfer curves of the OPT before (red) and after (blue) peeling off. d) Transfer characteristics of the OPT under dark and illumination conditions (λ = 810 nm), the inset figure shows the increased drain current in the accumulation region with the increased illumination intensity. e) Responsivity as a function of light intensity in the accumulation and depletion regions (λ = 810 nm). f) The noise spectrum of the OPT at $V_{gs} = -3$ V. All the measurements were carried under $V_{ds} = -3$ V.

The key component that enables the performance enhancement of our PPG sensor is its light detection unit. Our previous work has revealed that organic bulk heterojunction (BHJ)-based phototransistors can provide high responsivity through an electron-trapping induced photoconductive gain mechanism.[11] Here we adopted the phototransistor design for the PPG detection unit and selected a BHJ consisting of a narrow bandgap polymer, poly(*N*-alkyl diketopyrrolo-pyrrole dithienylthieno[3, 2-*b*]thiophene) (DPP-DTT), and a fullerene derivative, [6,6]-phenyl-C61-butyric acid methyl-ester (PCBM), as the active layer of the phototransistor.

We fabricated the bottom-gate bottom-contact configuration phototransistor on a silicon wafer coated with a 1.8 μm thick polyimide (PI) relief layer, which could serve as the substrate after delamination of the device from the silicon wafer. Solution-based PI was chosen as the relief material and device supporting layer due to its smooth surface, excellent thermal stability (glass transition temperature above 400 °C), good chemical resistance and weak adhesion to the silicon surface, which facilitate the lift-off of the phototransistor from the silicon supporting substrate. **Figure 1**a presents a schematic view of the organic phototransistor. A 30 nm thick gold (Au) gate electrode, a bilayer aluminum oxide(Al_2O_3, 50 nm)/silicon oxide (SiO_2, 10 nm) gate dielectric, 30 nm thick Au source/drain electrodes and a 80 nm thick semiconductor (DPP-DTT:PCBM) layer were sequentially formed on the PI substrate. The device fabrication procedures are shown in Figure S2 (Supporting Information), with the fabrication details described in the Experimental Section.

In the OPT, we used an Al_2O_3/SiO_2 bilayer dielectric to achieve low operating voltage. The Al_2O_3 layer, formed through atomic layer deposition (ALD), was chosen due to its high dielectric constant of 9. A thin layer of SiO_2 layer was sputtered on top of the Al_2O_3 layer to modify the surface chemistry of Al_2O_3. We found this modification layer is critical for achieving good transistor performance, presumably because the BHJ layer forms a better interface morphology on the octyltrichlorosilane (OTS) modified SiO_2 surface (see Figure S3a in the Supporting Information for the performance comparison of the devices with Al_2O_3 single layer dielectric and Al_2O_3/SiO_2 bilayer dielectric).

The areal capacitance of the bilayer dielectric was measured to be 60 nF cm^{-2}, allowing transistor operation at voltages below 3 V.

Since the PPG sensors will be brought into direct contact with human skin in practical applications, robust while mechanically flexible encapsulation is required to protect the phototransistor. Accordingly, we designed an encapsulation layer consisting of 200 nm thick polytetrafluoroethylene (PTFE) and 1.6 µm thick parylene C, in combine forming a sufficient barrier against diffusion of oxygen and water molecules. Moreover, the thickness of the encapsulation layer is matched with that of the polyimide substrate (both 1.8 µm). In this layout, the phototransistor is placed at the neutral mechanical plane (NMP), which helps to minimize the bending induced compressive and tensile strains on the device.[12] Electrical connections of the device with external circuits are done through anisotropic conductive film (ACF)-based interconnect wires. The encapsulated device exhibits almost the identical transfer characteristics before and after peeling off from the supporting Si substrate (Figure 1c) and the device performance remains stable after more than three months exposure in air (Figure S5, Supporting Information). These results demonstrate the effective mechanical and chemical protection enabled by the encapsulation layer.

We now evaluate the photodetection performance of the free-stranding OPT. Figure 1d shows the current–voltage characteristics of the OPT in dark and under NIR light (λ = 810 nm) illumination at different light intensities, based on which responsivity values are calculated and shown in Figure 1e. It can be seen that the responsivity increases with the decrease of light intensity in both accumulation and depletion modes, reaching its maximum at 3.5×10^5 A W^{-1} under 89 nW cm^{-2} illumination and at the gate voltage of $V_{gs} = -3$ V. The rise of responsivity at low light intensity indicates a transition from predominant band-to-band charge recombination (also referred as bimolecular recombination) to trap-assisted charge recombination at low charge carrier density, which often occurs in nanostructured photoconductive devices.[11,13] Such property is beneficial for PPG applications as the skin scattered or transmitted light signal is often weak.

To precisely evaluate the signal-to-noise ratio obtainable with a photodetector, the specific detectivity (D^*) or the noise equivalent power (NEP) of the device should be determined. NEP, the minimum impinging optical power that a detector can distinguish from the noise, is given as NEP = i_n/R, where i_n is the measured noise current in A Hz$^{-1/2}$ and R is the responsivity in A W^{-1}. The detectivity (D^*) can be calculated based on $D^* = (A\Delta f)^{1/2}/\text{NEP}$, where A is the device working area in cm^2 (≈0.5 mm^2 in our case) and Δf is the modulation frequency in the noise measurement in Hz.[14] The noise spectrum of the OPT is measured with an fast fourier transformation (FFT) spectrum analyzer, and it follows a typical $1/f$ pattern as shown in Figure 1f. Based on the noise current of 4.3×10^{-10} A Hz$^{-1/2}$ at 500 Hz and the responsivity of 3.5×10^5 A W^{-1} at 810 nm, we estimate that $D^* = 5.7 \times 10^{13}$ Jones (1 Jones = 1 cm Hz$^{1/2}$ W^{-1}) and NEP = 1.2×10^{-15} W Hz$^{-1/2}$, greatly surpassing the performance of commercially available silicon photodiodes, e.g., Model VTD34SMH from Excelitas Technologies with a detectivity of 5.7×10^{12} Jones and NEP of 4.8×10^{-14} W Hz$^{-1/2}$ at the maximum responsivity wavelength[15] and Model OPT101 from Texas Instruments with a NEP of 1.5×10^{-11} W Hz$^{-1/2}$[16] (note that lower NEP or higher detectivity means better photodetection performance). Finally, we also measured the temporal response of the phototransistor, and the result is shown in Figure S7 (Supporting Information). Based on the transient response of the device, the fall time of the photoresponse is around 0.6 ms, sufficiently fast to capture the arterial pulses.

Besides the use of the high sensitivity photodetector, we incorporate a high efficiency AlGaAs PN junction-based LED (power conversion efficiency: 14.3%) in the PPG sensor to further reduce the power assumption and heat dissipation of the entire system. Due to the small size (≈1 mm^2) of the LED chip, it does not affect much the conformal contact of the PPG sensor substrate with the skin. We have also developed a transfer printing process to fabricate and transfer ultrathin LED chips on skin, as described in the Supporting Information. Such process can be used when a seamless contact between the sensor and the skin is required.

For physiological monitoring we have designed and fabricated two types of NIR hybrid PPG (*h*PPG) sensors, disposable (epidermal) type and reusable (flexible) type. **Figure 2**a illustrates schematically the assembly process of the epidermal

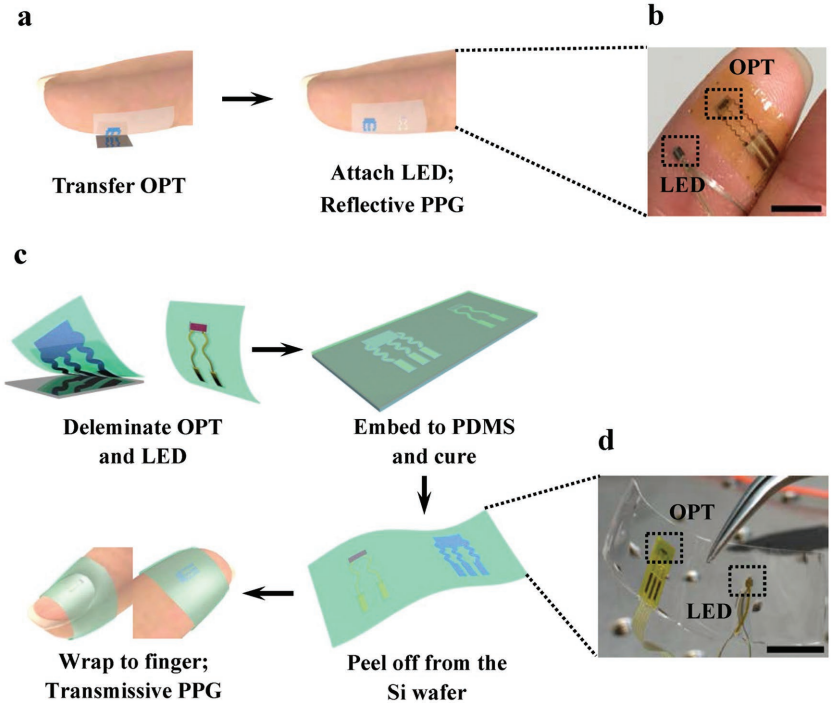

Figure 2. Epidermal and flexible hybrid organic/inorganic NIR PPG (*h*PPG). a) Illustration of the process flow for assembling the epidermal *h*PPG sensor. b) Photograph of a finger covered with the epidermal *h*PPG sensor (scale bar, 5 mm). c) Illustration of the process flow for assembly the flexible *h*PPG sensor. d) Photograph of the flexible *h*PPG sensor (scale bar, 10 mm).

*h*PPG sensor. In this approach, a thin (≈25 µm) stretchable acrylic adhesive[17] is attached on skin to facilitate the transfer printing process; then the OPT and LED are directly laminated onto the finger to form an epidermal reflection-mode *h*PPG sensor (Figure 2b). In this design, the elastomeric adhesive helps to bond the sensor tightly to skin, while the ultrathin geometry of the OPT significantly reduces the flexural rigidity and improves the bendability and degree of conformal contact with the skin.

In the second configuration, we have fabricated a bandage-like flexible *h*PPG sensor consisting of an OPT and a LED embedding into a 300 µm thick polydimethylsiloxane (PDMS) as a flexible substrate. The processing flow for sensor assembly is shown in Figure 2c, and the optical image of the sensor bandage is shown in Figure 2d. Here PDMS is selected as the substrate material due to its high flexibility and biomedical compatibility with skin tissue. The flexible bandage can be wrapped to a finger to form a transmission mode or reflection mode *h*PPG sensor, and it can be removed and reapplied for many times with little variation on the sensor performance (Figure S8, Supporting Information).

To demonstrate the practical application and accuracy of the two types of PPG sensors, we applied the sensors to perform measurements on cardiovascular parameters including HR, HRV, and BP.

For the HR and HRV measurements, we used the ECG signal of a human subject as the reference, and compared the performance of our epidermal *h*PPG sensor with a commercial reflection-mode PPG sensor (*c*PPG, assembled with a Model VSMG3700 LED and a Model VEMT4700 phototransistor from Vishay Semiconductors). The measurement layout of the ECG, *h*PPG, and *c*PPG sensors is shown in **Figure 3**a. The reliability of the HRV measurement is evaluated by comparing the sequence of the RR intervals (RRI) from the ECG signal and the peak-to-peak intervals from the PPG signals (note that ECG signal is regarded as a golden standard for detecting HRV[18]). Ten subjects were recruited in the experiment, and their PPG and ECG signals were collected for 1 min in a sitting position. The HR values calculated directly from the PPG and ECG signals, as well as the correlation of HRV between PPG and ECG sensors, are listed in Table S1 (Supporting Information), and the HRV tracking performance of a representative subject is shown in Figure 3b. It can be seen that the epidermal *h*PPG sensor well follows the instantaneous HR variations. The average correlation coefficient between *h*PPG-derived HRV and ECG-derived HRV is 0.88 for the 10 subjects. Furthermore, we observed only 0.3% error for the HR measurement when comparing the readings obtained from the epidermal *h*PPG sensor and the ECG sensor. Although *c*PPG still yields a higher correlation coefficient of 0.94 for HRV tracking (see the Supporting Information for detailed comparison), it consumes much higher peak power (≈20 mW) than the *h*PPG sensor (4 mW peak power).

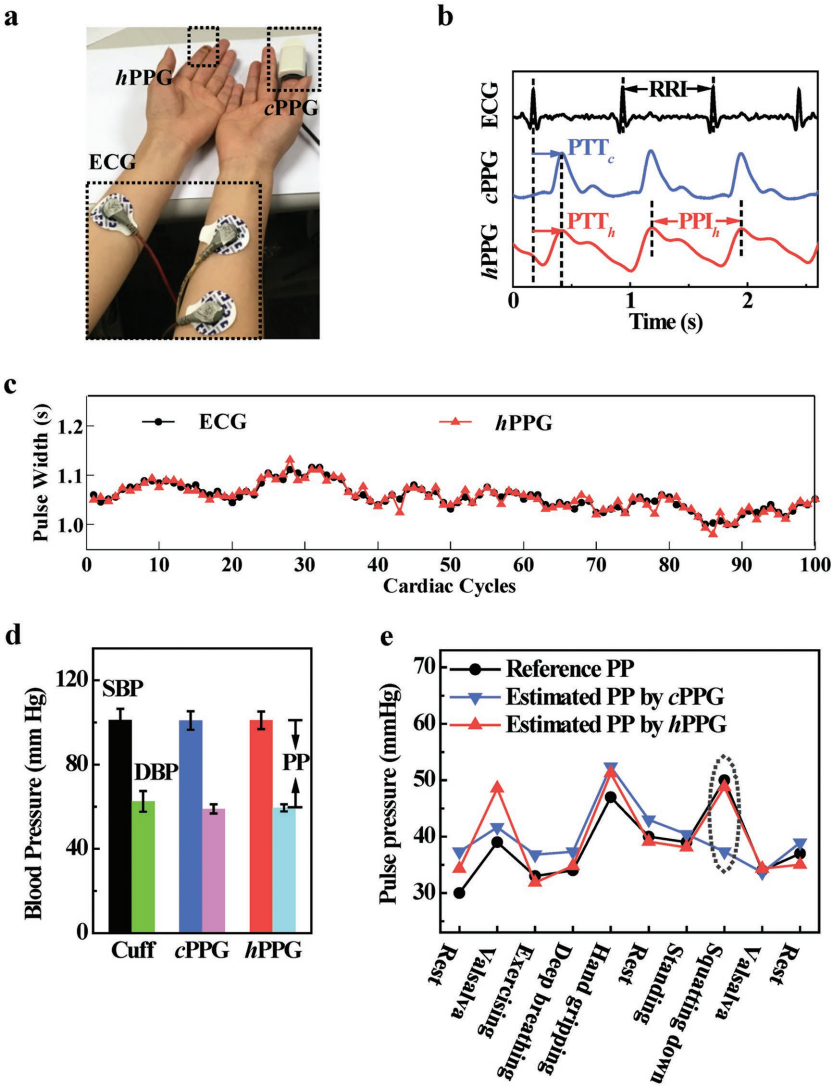

Figure 3. Monitoring of cardiovascular parameters using *h*PPG. a) Photograph of the measurement layout. b) Typical output signals measured by ECG, *c*PPG, and *h*PPG sensors, respectively, and illustration of the pulse transit time (PTT). c) HRV tracking performance on a representative subject. d) Cuffless systolic blood pressure (SBP) and diastolic blood pressure (DBP) calculated from the *h*PPG-ECG, *c*PPG-ECG; and the cuff-based values as reference. e) Variation of PP at different postures. Dashed circle highlights the position where *c*PPG cannot follow the PP change.

For the BP measurement, we extract the BP values based on the PPG and ECG signals using a pulse transit time (PTT) method, which is a widely used protocol for cuffless BP measurement.[19] The system measures ECG and PPG signals simultaneously, from which the PTT (defined as the time interval between the R wave peak of ECG and the peak of PPG[19]) of each cardiac cycle is determined, as illustrated in Figure 3b (note other characteristic points of PPG can be also used for

PTT calculation, like the trough or the maximum values of the first-order derivative of the PPG signal). The pulse wave velocity (PWV) in a blood vessel can be calculated based on the PTT using the Moens–Korteweg equation[20]

$$\mathrm{PWV} = \sqrt{\frac{Eh}{\rho d}} = \frac{L}{\mathrm{PTT}} \tag{1}$$

where E is the elastic modulus of a blood vessel, h is the blood vessel thickness, d is the arterial diameter, ρ is the blood density, L is the length of the blood vessel segment; PWV is inversely related to PTT. And BP can be related to PTT through E according to the Hughes equation[21]

$$\mathrm{E} = \mathrm{E}_0 \mathrm{e}^{\alpha \mathrm{P}} \tag{2}$$

Where E_0 is the elastic modulus at zero pressure, $\alpha \approx 0.017$ mm Hg^{-1}, and P is the mean blood pressure. Therefore, with an initial calibration under the assumption that vessel thickness and diameter keep constant, PTT can be translated to BP through a logarithmic relation: $P = k\ln\mathrm{PTT} + b$. Systolic blood pressure (SBP) and diastolic blood pressure (DBP) can be estimated according to the following equations[19a]

$$\begin{aligned} \mathrm{DBP} &= \frac{\mathrm{SBP}_0}{3} + \frac{2\mathrm{DBP}_0}{3} + A\ln\left(\frac{\mathrm{PTT}_0}{\mathrm{PTT}}\right) - \frac{(\mathrm{SBP}_0 - \mathrm{DBP}_0)}{3}\frac{\mathrm{PTT}_0^2}{\mathrm{PTT}^2}, \\ \mathrm{SBP} &= \mathrm{DBP} + (\mathrm{SBP}_0 - \mathrm{DBP}_0)\frac{\mathrm{PTT}_0^2}{\mathrm{PTT}^2} \end{aligned} \tag{3}$$

where PTT_0 is the initial PTT of the first recorded cardiac cycle, and A is a subject-dependent coefficient but can be approximated for a population.[21] Thereupon, pulse pressure (PP), the difference between SBP and DBP, can be estimated through the equation[22]

$$\mathrm{PP} = \mathrm{PP}_0\frac{\mathrm{PTT}_0^2}{\mathrm{PTT}^2} = (\mathrm{SBP}_0 - \mathrm{DBP}_0)\frac{\mathrm{PTT}_0^2}{\mathrm{PTT}^2} \tag{4}$$

The PTT method requires a one-time calibration procedure to map PTT to BP, where a standard clinical device (e.g., a sphygmomanometer) together with a cuffless BP sensor system is applied to determine the initial SBP_0 and DBP_0 of a subject.

To compare our flexible *h*PPG-based cuffless BP measurement unit with commercial PPG (*c*PPG)-based devices, we measured the subjects' ECG, *h*PPG, and *c*PPG signals at different postures of a subject. The beat-to-beat BP values were calculated from *h*PPG/ECG and *c*PPG/ECG signal combinations according to Equation (3). Figure 3d shows the average beat-to-beat SBP and DBP values calculated based on the PTT values extracted from Figure 3c. It can be seen that the average values of *h*PPG/ECG-based SBP and DBP are consistent with those obtained from the *c*PPG/ECG setup. Furthermore, the average SBP and DBP show <5 mm Hg mean absolute difference with the reference readings provided by the commercial cuff-based device (OMRON), confirming the accuracy of the measurements.

The advantage of our flexible *h*PPG sensor becomes evident when we compare the measured PP of a subject at different postures, according to Equation (4). PP, which represents the pulsatile component of blood flow, normally increases with aging and loss of arterial elasticity, and thus has been suggested as an predictor of CVDs in general population. As shown in Figure 3e, the PP value varied with the transitions of the subject's postures. The mean absolute differences between the PPG measured values and the reference values are 2.5 and 4.2 mm Hg for *h*PPG-based and *c*PPG-based systems, respectively. Furthermore, the *h*PPG-based system shows better tracking capability as highlighted in Figure 3e. Note however that the accuracy of the PTT estimation on DBP could vary from subject to subject. Therefore to fully validate the new PPG device for PP tracking, the experiment should be performed on an adequate size (ideally above 30) of subjects.

In conclusion, we have developed epidermal and flexible PPG sensors that can be operated in the near-infrared regime with high sensitivity and low power consumption. The excellent sensor performance is achieved through development of a low-voltage driven and high detectivity organic bulk heterojunction phototransistor and through incorporation of the phototransistor into a well encapsulated, highly flexible, and transfer-printable device configuration. We have demonstrated that the epidermal/flexible PPG sensors are capable of continuously monitoring HRV and precisely tracking the changes of PP at different postures of human subjects with the aid of ECG monitoring, exhibiting more reliable performance than conventional PPG sensors while consuming less power. The study suggests that the hybrid PPG sensor design may provide a promising solution for low-power, real-time physiological monitoring and thus benefit the prognosis and diagnosis of cardiovascular diseases.

Experimental Section

Organic Phototransistor: A schematic description of the fabrication processes is shown in Figure S1 (Supporting Information). First, a 1.8 µm thick PI layer, which was to be used as the substrate after delamination, was formed by spin coating (3300 rpm, 45 s) poly(pyromellitic dianhydride-co-4,4′-oxydianiline), amic acid solution (Sigma-Aldrich) on a supporting Si wafer, followed by curing at 250 °C for 1 h at atmosphere. Then, Cr/Au (3/30 nm), which serves as gate electrode, was deposited via thermal evaporation through a shadow mask onto the PI. The bilayer gate dielectric Al_2O_3/SiO_2 (50/10 nm) was deposited by ALD and by sputtering, respectively. The gate dielectric was patterned by etching in buffered oxide etchant (6:1). On top of the gate dielectric, Cr/Au (3/30 nm) source-drain electrodes were defined by photolithography to get a channel length of 5 µm and channel width of 15 mm. The substrate with dielectric and electrodes was treated with oxygen plasma for 40 s, and first immersed in 0.1 M solution of octyltrichlorosilane (OTS-8, Sigma-Aldrich) in n-hexane at 60 °C for 30 min, then immediately immersed in 10×10^{-3} M solution of 1-octanethiol (Sigma-Aldrich) in isopropanol for 5 min at room temperature. After thoroughly rinsing the substrate with isopropanol and drying under a nitrogen flow, the photosensitive semiconductor solution comprising of a 2:1 mass ratio of DPP-DTT (synthesized as previously described[23]):PCBM (Sigma-Aldrich) dissolved to 8 mg mL^{-1} in 1,2-dichlorobenzene was spin coated (2500 rpm, 120 s) and annealed at 135 °C for 10 min under nitrogen environment, resulting in a 80 nm thick film. Finally, the entire device was then encapsulated with a bilayer of PTFE/Parylene C (200 nm/1.8 µm) to position near the NMP. The PTFE layer was formed by spin coating (800 rpm, 60 s) Teflon AF (400S2-100-1, 1% solution, DuPont) and annealed at 80 °C for 10 min in a nitrogen atmosphere, and the Parylene C layer was deposited by

CVD. After the fabrication process, the contact pads for source/drain and gate electrodes were bonded to an ACF (Elform, P/N: HST-9805-210). The entire device was then peeled off from the supporting Si wafer and subjected to device characterization.

The current–voltage characteristics were measured in air with a Keithley 2612 Source Meter both in the dark and under illumination conditions by a NIR (810 nm) laser with neutral density filters (Thorlabs Inc.).

The dark current noise i_n measurement was performed at room temperature with the model SR760 FFT spectrum analyzer.

Inorganic Light-Emitting Diode: NIR LED chips (810 nm) (Model ED-B42IRT-RS) were purchased from OPTOTECH and bonded to ACF cables for power supplies. The thinning process of the chips is illustrated in the Supporting Information.

Hybrid PPG Sensors: Epidermal *h*PPG sensor was assembled by directly laminating the OPT and OPD onto the left index finger using 25 µm acrylic adhesive (3 M).

Sylard 184 PDMS (Dow corning) was used for integrating flexible *h*PPG sensor. The flexible *h*PPG sensor was fabricated by embedding the OPT and LED in the prepolymer mixture of PDMS spin coated on a Si wafer. After curing, the *h*PPG sensor bandage was peeled off from the Si wafer, and wrapped around the left index finger.

Cardiovascular Parameters Monitoring: The *h*PPG sensor was attached on the left index finger. In the experiment, the LED was powered by a 1.5 V battery, and the OPT data were collected using $V_{ds} = -3$ V, $V_{gs} = 3$ V. The recording of the OPT was performed using a Keithley 2612 Source Meter and customized Labview software. At the same time, an ECG electrode was places on the left forearm of the subject, another two ECG electrodes were placed on the right forearm the subject; and as a comparison, a reflection-mode *c*PPG sensor was clipped to the right index finger of the subject. Note that although the fingertip position is the most common one for PPG measurement and PTT-based BP extraction, there may be other body locations, e.g., wrist, that can provide better signals to the sensor for physiological monitoring. The ECG and *c*PPG signals were recorded and display on the PC through a DAQ (DI-720-USB, 14-bit analog to digital conversion, DATAQ Instruments). For comparison, the *h*PPG, ECG, and *c*PPG signals were recorded simultaneously.

Supporting Information

Supporting Information is available from the Wiley Online Library or from the author.

Acknowledgements

This work was supported by the Innovation and Technology Fund (Ref. No: ITS/111/14) from the Innovation and Technology Commission of Hong Kong and The Chinese University of Hong Kong grant (Ref. No: 3132823). The authors would like to thank Dr. Mengyu Chen for her assistance in photoresponse characterization. The authors would also like to thank the volunteer subjects for their participation in the physiological signal measurements.

Conflict of Interest

The authors declare no conflict of interest.

Keywords

near-infrared, organic/inorganic hybrids, organic phototransistors, photoplethysmogram sensors

Received: February 17, 2017
Revised: April 6, 2017
Published online: June 14, 2017

[1] W. B. Kannel, C. Kannel, R. S. Paffenbarger, L. A. Cupples, *Am. Heart J.* **1987**, *113*, 1489.
[2] a) M. T. La Rovere, J. T. Bigger, F. I. Marcus, A. Mortara, P. J. Schwartz, *Lancet* **1998**, *351*, 478; b) H. Tsuji, M. G. Larson, F. J. Venditti, E. S. Manders, J. C. Evans, C. L. Feldman, D. Levy, *Circulation* **1996**, *94*, 2850.
[3] a) S. MacMahon, R. Peto, R. Collins, J. Godwin, S. MacMahon, J. Cutler, P. Sorlie, R. Abbott, R. Collins, J. Neaton, R. Abbott, A. Dyer, J. Stamler, *Lancet* **1990**, *335*, 765; b) W. B. Kannel, *JAMA, J. Am. Med. Assoc.* **1996**, *275*, 1571.
[4] http://www.who.int/cardiovascular_diseases/en/ (accessed: December 2016).
[5] a) J. Kim, G. A. Salvatore, H. Araki, A. M. Chiarelli, Z. Xie, A. Banks, X. Sheng, Y. Liu, J. W. Lee, K. Jang, S. Y. Heo, K. Cho, H. Luo, B. Zimmerman, J. Kim, L. Yan, X. Feng, S. Xu, M. Fabiani, G. Gratton, Y. Huang, U. Paik, J. A. Rogers, *Sci. Adv.* **2016**, *2*, e1600418; b) C. M. Lochner, Y. Khan, A. Pierre, A. C. Arias, *Nat. Commun.* **2014**, *5*, 5745; c) T. Yokota, P. Zalar, M. Kaltenbrunner, H. Jinno, N. Matsuhisa, H. Kitanosako, Y. Tachibana, W. Yukita, M. Koizumi, T. Someya, *Sci. Adv.* **2016**, *2*, e1501856; d) A. K. Bansal, S. Hou, O. Kulyk, E. M. Bowman, I. D. W. Samuel, *Adv. Mater.* **2015**, *27*, 7638.
[6] a) S. Lu, H. Zhao, K. Ju, K. Shin, M. Lee, K. Shelley, K. H. Chon, *J. Clin. Monit. Comput.* **2008**, *22*, 23; b) Y. L. Zheng, X. R. Ding, C. C. Y. Poon, B. P. L. Lo, H. Zhang, X. L. Zhou, G. Z. Yang, N. Zhao, Y. T. Zhang, *IEEE Trans. Biomed. Eng.* **2014**, *61*, 1538.
[7] a) G. Schwartz, B. C. Tee, J. Mei, A. L. Appleton, D. H. Kim, H. Wang, Z. Bao, *Nat. Commun.* **2013**, *4*, 1858; b) N. Luo, W. Dai, C. Li, Z. Zhou, L. Lu, C. C. Y. Poon, S.-C. Chen, Y. Zhang, N Zhao, *Adv. Funct. Mater.* **2016**, *26*, 1178.
[8] Y. Chuo, B. Omrane, C. Landrock, J. N. Patel, B. Kaminska, *IEEE Sens. J.* **2010**, 155.
[9] J. Spigulis, L. Gailite, A. Lihachev, R. Erts, *Appl. Opt.* **2007**, *46*, 1754.
[10] S. Wang, X. Yan, Z. Cheng, H. Zhang, Y. Liu, Y. Wang, *Angew. Chem., Int. Ed.* **2015**, *54*, 13068.
[11] H. Xu, J. Li, B. H. K. Leung, C. C. Y. Poon, B. S. Ong, Y. Zhang, N. Zhao, *Nanoscale* **2013**, *5*, 11850.
[12] T. Sekitani, S. Iba, Y. Kato, Y. Noguchi, T. Someya, T. Sakurai, *Appl. Phys. Lett.* **2005**, *87*, 173502.
[13] G. Konstantatos, M. Badioli, L. Gaudreau, J. Osmond, M. Bernechea, F. P. G. De Arquer, F. Gatti, F. H. L. Koppens, *Nat. Nanotechnol.* **2012**, *7*, 363.
[14] G. Konstantatos, I. Howard, A. Fischer, S. Hoogland, J. Clifford, E. Klem, L. Levina, E. H. Sargent, *Nature* **2006**, *442*, 180.
[15] http://www.excelitas.com/downloads/dts_vtd34sm.pdf (accessed: December 2016).
[16] http://www.ti.com/lit/ds/symlink/opt101.pdf (accessed: February 2017).
[17] J. Kim, A. Banks, H. Cheng, Z. Xie, S. Xu, K. I. Jang, J. W. Lee, Z. Liu, P. Gutruf, X. Huang, P. Wei, F. Liu, K. Li, M. Dalal, R. Ghaffari, X. Feng, Y. Huang, S. Gupta, U. Paik, J. A. Rogers, *Small* **2015**, *11*, 906.
[18] M. Malik, A. J. Camm, J. T. Bigger, G. Breithardt, S. Cerutti, R. J. Cohen, P. Coumel, E. L. Fallen, H. L. Kennedy, R. E. Kleiger, F. Lombardi, A. Malliani, A. J. Moss, J. N. Rottman, G. Schmidt, P. J. Schwartz, D. H. Singer, *Eur. Heart J.* **1996**, *17*, 354.
[19] a) C. C. Y. Poon, Y. T. Zhang, *Conf. Proc. IEEE Eng. Med. Biol. Soc.* **2005**, *6*, 5877; b) B. M. McCarthy, B. O'Flynn, A. Mathewson, *J. Phys.: Conf. Ser.* **2011**, *307*, 12060.
[20] J. C. Bramwell, A. V. Hill, *Proc. R. Soc. B* **1922**, *93*, 298.
[21] D. J. Hughes, C. F. Babbs, L. A. Geddes, J. D. Bourland, *Ultrason. Imaging* **1979**, *1*, 356.
[22] X.-R. Ding, Y.-T. Zhang, J. Liu, W.-X. Dai, H. K. Tsang, *IEEE Trans. Biomed. Eng.* **2016**, *63*, 964.
[23] J. Li, Y. Zhao, H. S. Tan, Y. Guo, C.-A. Di, G. Yu, Y. Liu, M. Lin, S. H. Lim, Y. Zhou, H. Su, B. S. Ong, *Sci. Rep.* **2012**, *2*, 754.

